

Failure Analysis of 316L Air Cooler Stainless Steel Tube in a Natural Gas Production Field

A. Bahgat Radwan¹, Aboubakr M. Abdullah^{*,1}, Hans J. Roven^{1,2}, Adel M. Mohamed^{*,1,3}, Mobbassar Hassan SK¹

¹Center for Advanced Materials, Qatar University, Doha 2713, Qatar

² Department of Materials Science and Engineering, Norwegian University of Science and Technology, 7491 Trondheim, Norway

³ Department of Metallurgical and Materials Engineering, Faculty of Petroleum and Mining Engineering, Suez University, Box 43721, Suez, Egypt

*E-mail: abubakr_2@yahoo.com, adel.mohamed25@yahoo.com,

Received: 14 May 2015 / *Accepted:* 8 July 2015 / *Published:* 28 July 2015

In spite of the excellent resistance of stainless steel (SS) towards uniform corrosion, overcoming various localized corrosion could be a real challenge. This work presents an analysis of the failure behavior of 316L SS air chiller tube with a peripheral crack used in a Qatari gas company in Qatar. Macroscopic failure characteristics were analyzed by means of visual inspection, digital imaging while light microscopy, electron microscopy (SEM / EDX), and X-ray fluorescence (XRF) were employed for microstructural and fractographic characterization. The results indicate that the failure phenomenon that was primarily initiated by CI led to an eventual autocatalytic pitting corrosion. The failure reasons of the tube are related to the combined effect of constant and cyclic external stresses, as well as internal residual stress originated from various operating conditions.

Keywords: Failure analysis; stainless steel; inclusions; pitting corrosion; fractography

1. INTRODUCTION

As a source of clean energy, natural gas has been used extensively for heating, cooking and fueling. The demand for natural gas is expected to increase by up to 53% of the energy consumption by 2020 [1]. Gas and oil liquefaction and distribution through pipelines demands high level of safety, cost reduction and operational efficiency increase. Nearly 40% of the pipeline networks around the world have reached the end of their projected life span [1].

The type and magnitude of the corrosion damages that may take place in the industrial gas facility are mainly depending on type of environments, concentration of the contaminants, and the operating conditions of the pipelines. For instance, gas' temperature and velocity in the pipeline play an important role in detecting whether corrosion will take place and where it might happen. In other words, a particular gas composition may induce corrosion under some operating conditions but not in others.

The presence of chloride is one of the main factors that induce local corrosion. Many approaches studied their effect on pitting corrosion [2-4]. Most of authors proposed Cl^- ions' adsorption on the metal surface which leads to a passivity breakdown. Corrosion-fatigue can take place in all metallic materials subjected to an aggressive environment, particularly Cl^- ions, and exposed to fatigue stress. In the view of fatigue and stress corrosion cracking (SCC), there are variable faces of the problem originated from metallurgical, mechanical and environmental properties [5, 6].

The failure analysis of 316L SS has been investigated in different environments in order to identify the main reasons of failure and thus participates in the enhancements of the operation and performance of similar structure under the same conditions. For example, in a Saudi petrochemical plant, 316L SS burner tubes of an ethylene cracking furnace failed prematurely and repeatedly due to chloride stress corrosion cracking (CLSCC) [7]. 316L SS bellows of a pressure safety valve of a petroleum refinery failed within a time span of one week due to CLSCC [8]. Also, the existence of sulfide inclusions participated in fatigue fracture of 316L SS in Brazilian petroleum refinery [9].

The combination of cyclic stresses, which is correlated to an intermittent operational mode, and stress concentration at the base of a fillet weld around internal welding defects result in failure of duplex stainless steel in a natural gas production field [10].

Different kinds of mechanisms can be utilized in order to explore the main reasons of failure in structures or equipment. Communally, the reasons are elated to the usage of in appropriate materials, the existence of faults, design errors, unsuitable assembly, or inappropriate conditions through usage. Information about the reasons and the repairing of the defects permit enhancing the performance of similar material and avoid the repetition of the similar type of failure [11]. Frequently, scanning electron microscope (SEM) has been utilized for failure analysis to relate the morphology of the fracture surface to the potential reasons of fracture [12].

The purpose of this work was undertaken to study an industrial case regarding the failure behavior of 316L SS air chiller tube supplied by a Qatari Gas Company. Macroscopic failure characteristics of the specimens were examined using SEM and XRF techniques.

2. EXPERIMENTAL

In this work a detail failure analysis of 316L SS air cooler from a Qatari Gas company with a peripheral crack at the edge of the roll expansion close to the clamping area is performed. Figure 1 shows photograph of the as received failed 316L stainless steel tube connected to the cooler pipe.



Figure 1. Overview of the as-received failed tube connected to the cooler pipe. Arrows refer to the inspected regions.

The chemical composition of the failed air cooler tube 316L SS was inspected by spark emission spectrometer 3460-D-UVU. Table 1 lists the chemical composition of 316Lstainless.

The operating temperature and pressure at the cracked region of the tube were $50^{\circ}\pm 5$ and 27 bar, respectively. The gas is composing of alkanes C1- C5. The cracked 316 L stainless steel neck in the delivered air cooler was analyzed to determine the failure mechanism.

Table 1. The chemical composition of 316L stainless steel tube (wt%)

Element	The Element Max. (wt%)	Failed 316L SS tube (wt%)
C	0.03	0.02
Mn	2.00	1.5
P	0.045	0.06
S	0.03	0.13
Si	0.75	0.92
Cr	16.0-18.0	18
Ni	10.0-14.0	9.47
Mo	2.00-3.00	2
N	0.10	--

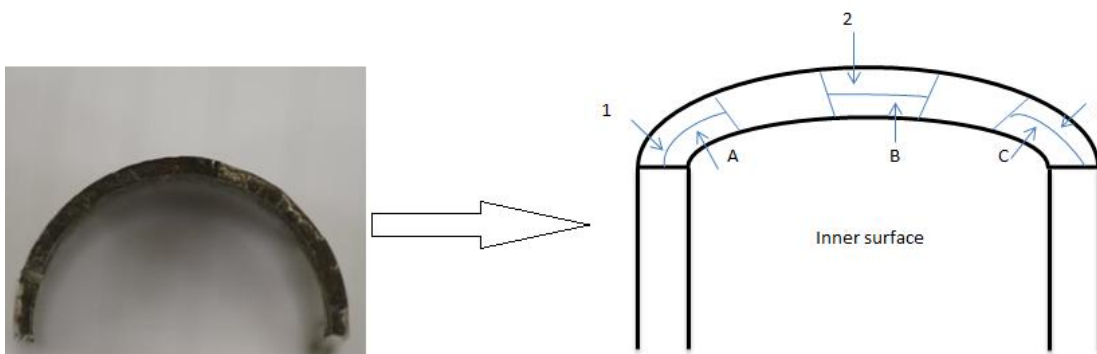


Figure 2. Schematic macrograph for the investigated areas at the fracture surface of 316L SS tube.

At the outer surface of the tube (exactly behind the crack) a horizontal cross section parallel to the crack propagation plane was done without touching the crack surface, as shown in Figure 2. The test locations are indicated by arrows as shown in Figure 2. In other words, the fracture surface has been divided into six sections, the three alphabets sections are closed to the inner surface exposed to the gas (A, B and C) and the other three numerical sections are closed to the outer surface. The length of each inspected section is 10 mm.

The morphology and fractography have been investigated using field-emission scanning electron microscope (SEM, FEI NOVA NANOSEM 450, Netherlands). SEM images were taken from six different places of the fracture surface to study the form of corrosion. The fractured surface's diameter is 50 mm and the length of each inspected arc is 10 mm length.

In Figure 2, regions A, B and C show the SEM images taken from the inner surface which was in contact with the processed gas and regions 1, 2 and 3 show the SEM images of the outer surface. Fry's Reagent Etching techniques per ASTM standard E. 407 as No. 79 revealed the microstructure.

3. RESULTS AND DISCUSSION



Figure 3. Photograph image for the crack region of 316L SS tube.

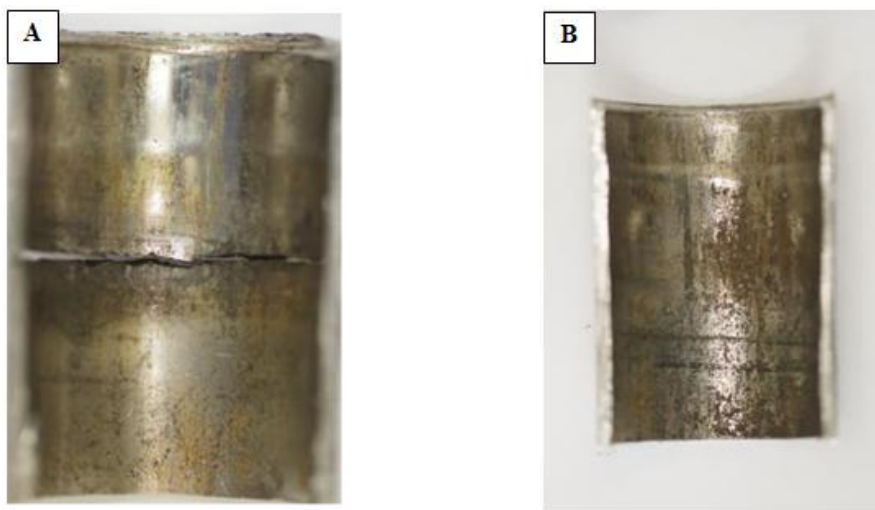


Figure 4. [A and B]. Show the inner cross section of 316L SS tube after cutting.

Visual examination of the cracked tube section was performed by naked eye and a digital camera before and after cutting. Digital imaging of the fracture surface clearly revealed the crack was localized at the center of tube and adjacent to the clamping area, as shown in Figure 3 .

The sectioned sample showed accumulation of corrosion products at the inner surface which was even denser at the outer side, as illustrated in Figure 4 [A and B]. Correspondingly, the fracture surface at the central region showed a deep dark color (pointed out in Figure 5), which was more intense and closed to the inner surface, as depicted in Figure 2 [A, B and C]. However, the black tint diminished in magnitude towards the ends of the crack area, see the regions 1, 2 and 3 in Figure 2. A release of the pronounced internal stresses was noticed during the cutting of the tube e.g. sudden brittle failure occurred and the part fell into several pieces although the cutting was done ca. 1cm apart from the failure.



Figure 5. Overview of the fracture surface of 316L SS tube showing heavy oxidized regions (deep dark color) and less oxidized places (light color).

According to the ASTM A-240 standard the limit sulfide content should not override 0.03%, see Table 1. The XRF analysis however pointed out that, the sulfide content is much more than the upper limit determined by the standard (0.16 %). Sulfur has a detrimental role in the degradation of the mechanical properties of stainless steels [13]. Since sulfide inclusions aligned on the rolling direction are the reasons of mechanical anisotropy and low corrosion resistance, therefore it is substantial to reduce the sulfur content below 0.020% especially in applications which demand high toughness and ductility [14].

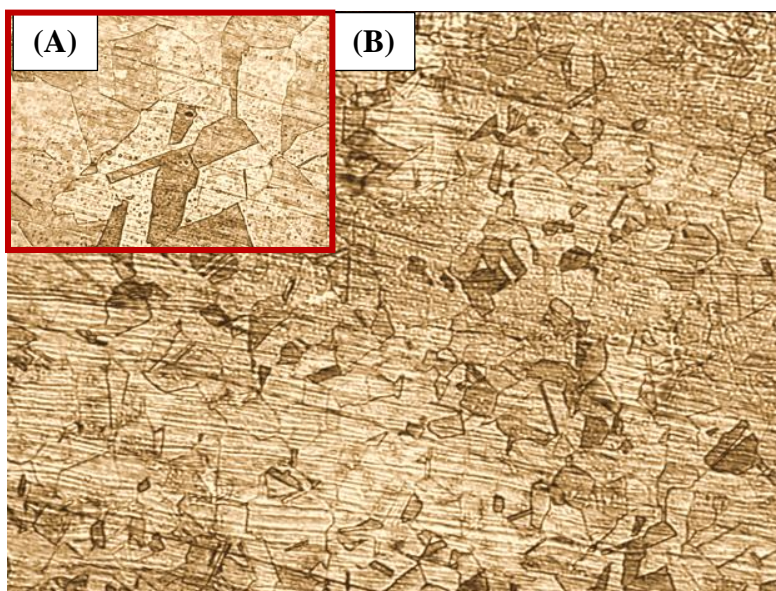


Figure 6. Optical microstructure of 316L SS air cooler tube using Fry's reagent at (A) 50X and (B) 10X magnifications.

Figure 6 shows the microstructure of 316L stainless steel. The average size of the austenitic grains (austenitic isles in a continuous matrix of ferrite) is about 30 μm which is reasonable in case of 316L stainless steel. It may be observed that different types of corrosion induced by Cl^- resulted in failure of the tub. The first type is chloride induced fatigue cracking corrosion due to internal cyclic stress, resulted in ductile fracture. The second type is chloride induced stress cracking corrosion under constant external stress (due to clamping around air cooler tube circumference). Chloride ions accumulate locally at the regions at stress concentration and induce the initiation of a crack. The combined effects of these corrosion types led to the final failure of 316L SS.

Figure 7 illustrates that the actual corrosion event initiated at the inner surface and was followed by subsequent cleavage occurring at the outer surface which led to the ultimate failure of stainless steel tube.

The first corrosion type occurred as result of interaction of Cl^- ions with manganese sulfide (MnS) inclusions, which acts as active sites for initiation of corrosion pits, see Figure 8 (A and B). Dissolution of inclusions were noticed and proposed to be the first step for pit formation [15, 16]. This proposed mechanism originated from the presence of Mn, where it segregates sulfur as MnS instead of

FeS (thermodynamically unstable and low melting phase) in order to attain a system with higher degree thermodynamic stability and melting point.

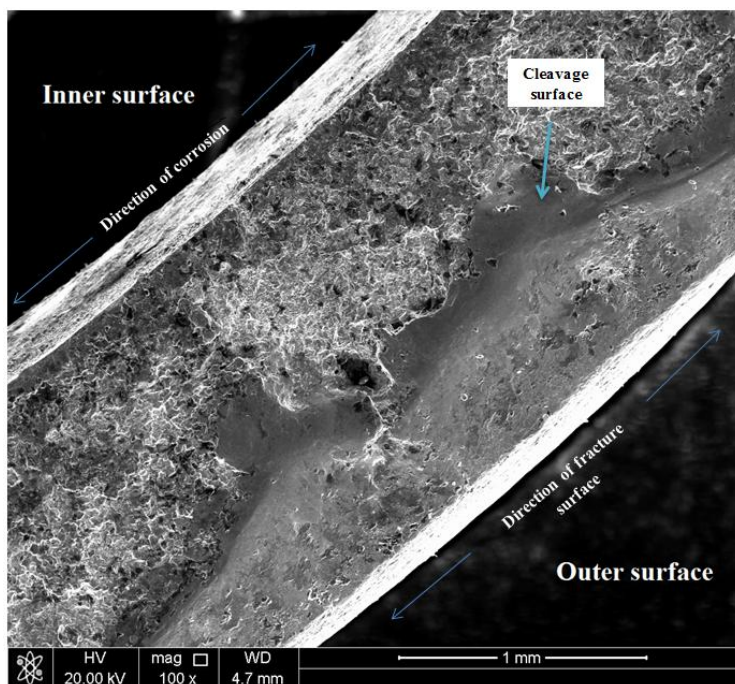
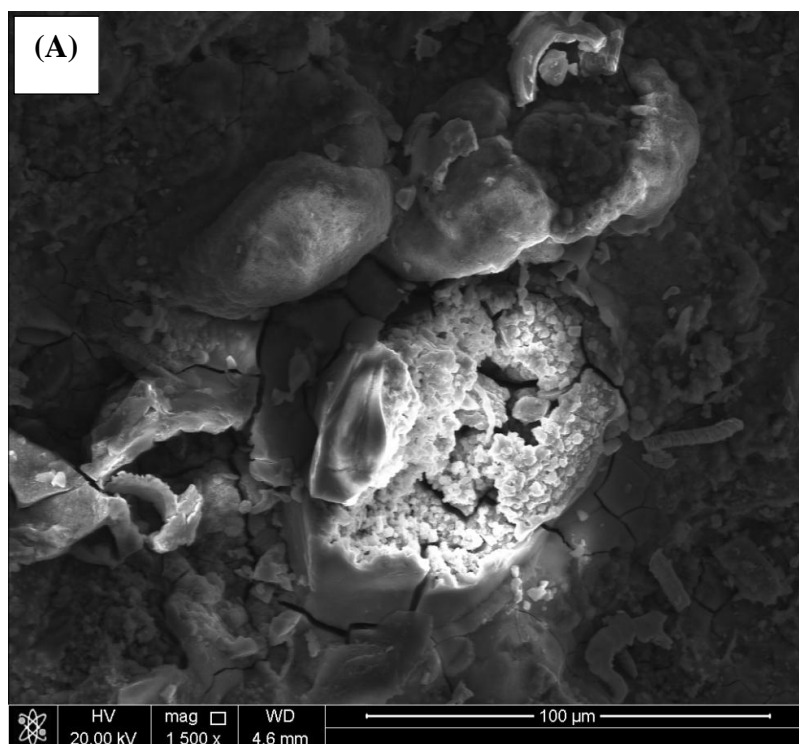


Figure 7. SEM micrograph at low magnification showing the cracking corrosion of inner surface and cleavage fracture at outer surface.



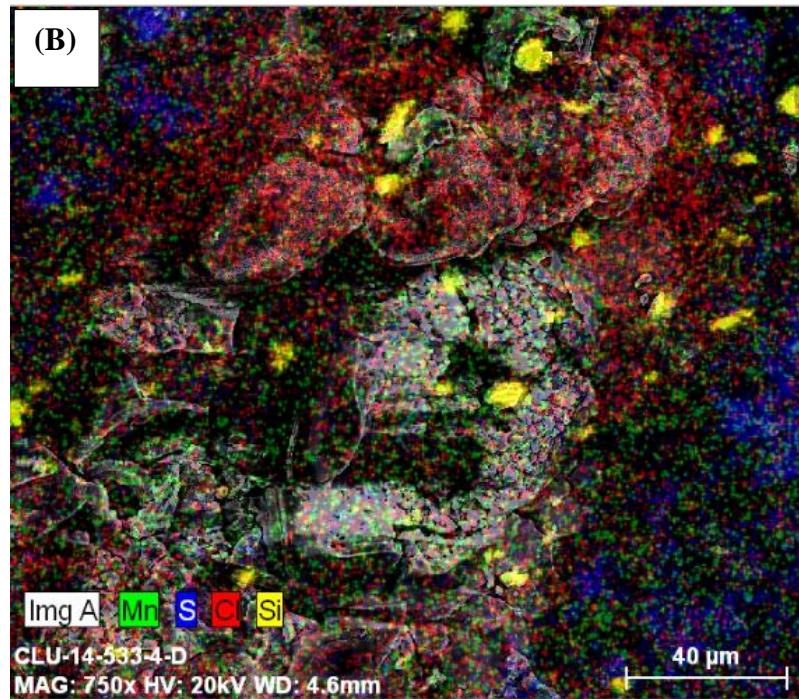


Figure 8. (A) The initiation of pits formation due to MnS inclusion on the inner surface of 316L stainless steel and (B) the corresponding EDX mapping image.

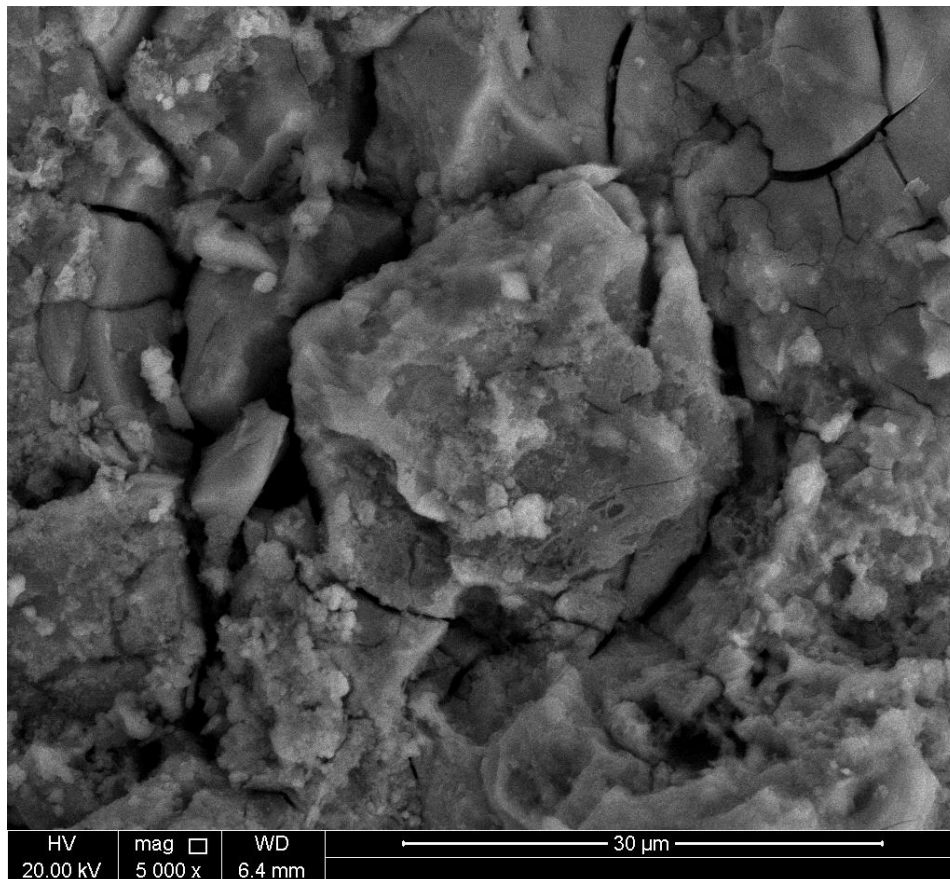


Figure 9. Typical SEM micrograph of the corrosion- fatigue fracture on the outer surface of 316L stainless steel tube.

Eklund [17], however, non-metallic inclusions in austenitic stainless steel (and the most detrimental among them is sulfide inclusions such as MnS) are responsible for pitting initiation. Wranglén [18], also reported similar results regarding the role of MnS in pitting initiation of stainless steel. Stewart and Williams' work [19] in dilute neutral chloride solutions, also confirmed similar conclusion regarding sulfide inclusions. They used electrochemical and microstructural characterization to prove that pits are initially formed at the sulfur-rich inclusions in 304L SS.

Intergranular corrosion fatigue cracks, as illustrated in Figure 9, are presumably as a result of cyclic stresses. Figure 10 shows the formation of microcracks at the inclusion sites where the pits were formed and their subsequent propagation from the base of pits. This observation is in agreement with the most common mechanism of crack initiation and propagation due to corrosion fatigue as suggested by Butler and Isom [20].

Different regimes have been suggested to clarify the corrosion fatigue behavior [21, 22]. Bayoumi [23], indicated that the endurance of chloride induced fatigue corrosion arises through incorporation of both environmental factor and applied cyclic stresses. Many researchers have reported pitting as an important element in corrosion and thereby in corrosion fatigue cracking of materials containing second phase particles [24] and consequently, resulted in the formation of micro-cracks (at/around the location of an inclusion), as an evident in Fig. 10.

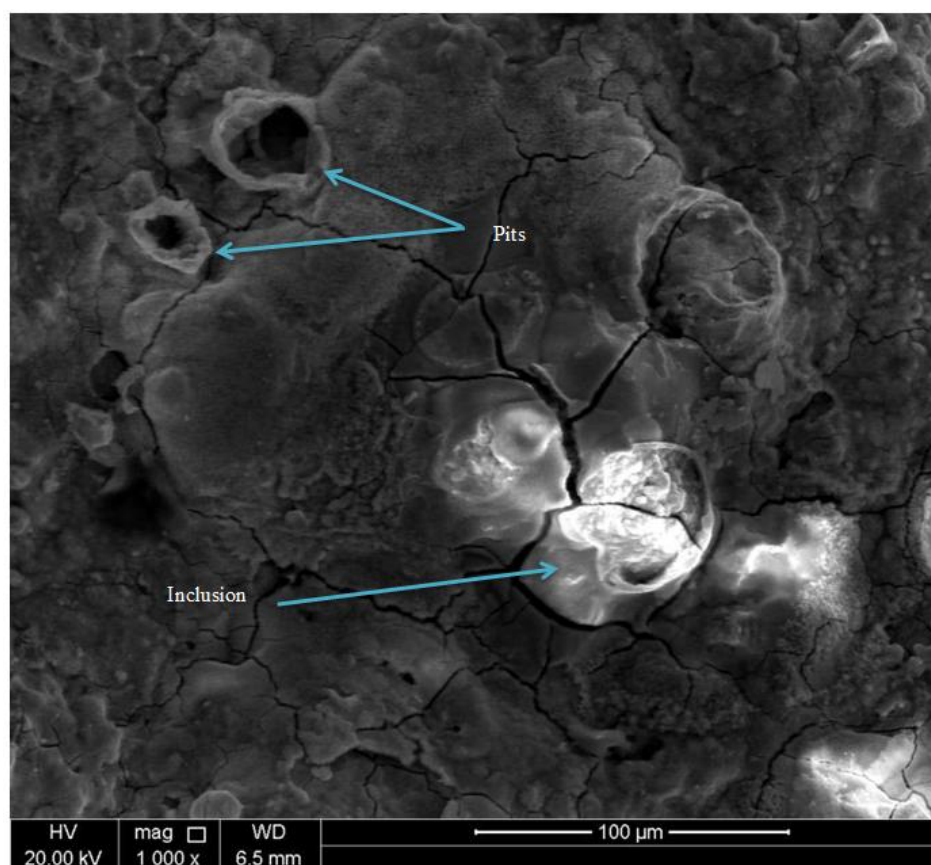


Figure 10. SEM micrograph showing the formation of stress cracking corrosion around of pits on outer surface of 316L SS air cooler tube.

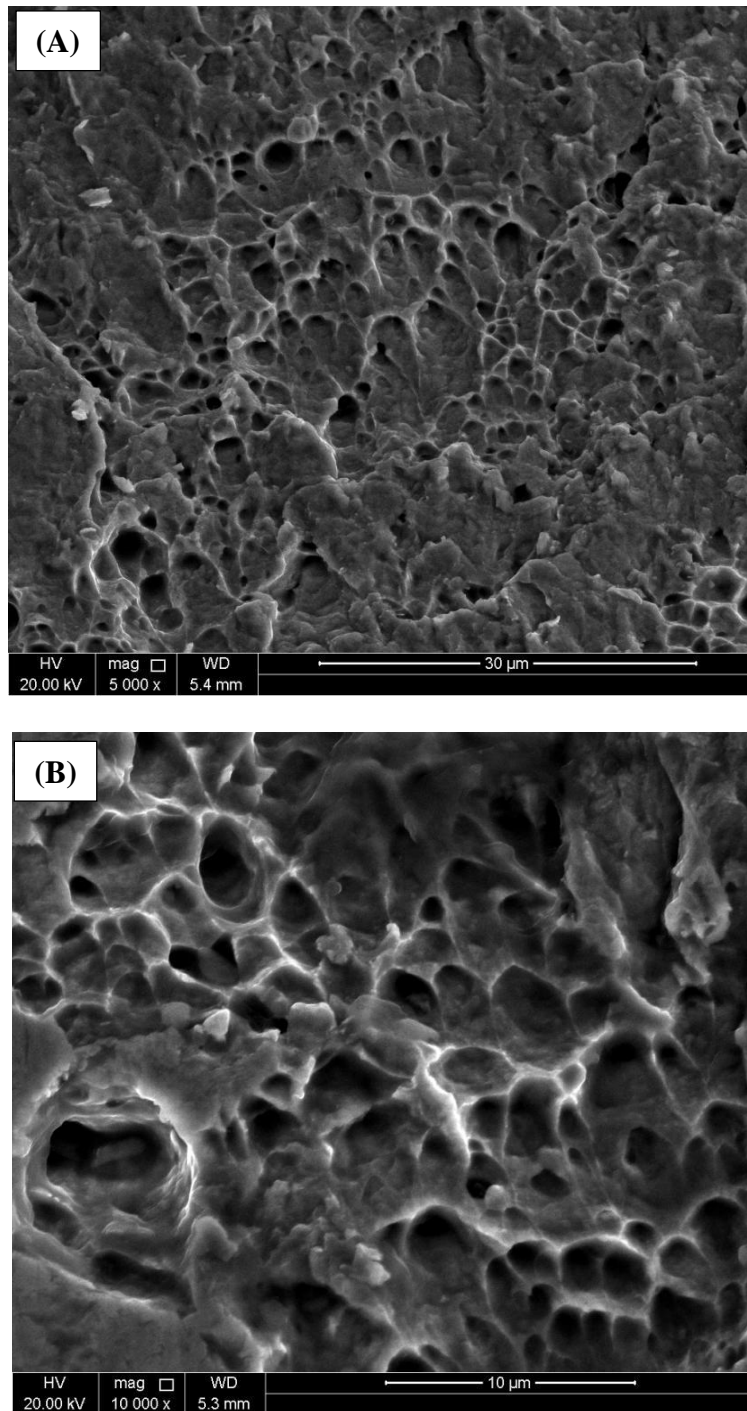


Figure 11 [A and B]. Fractography of the ductile fracture on the outer surface of 316L stainless steel at different magnifications.

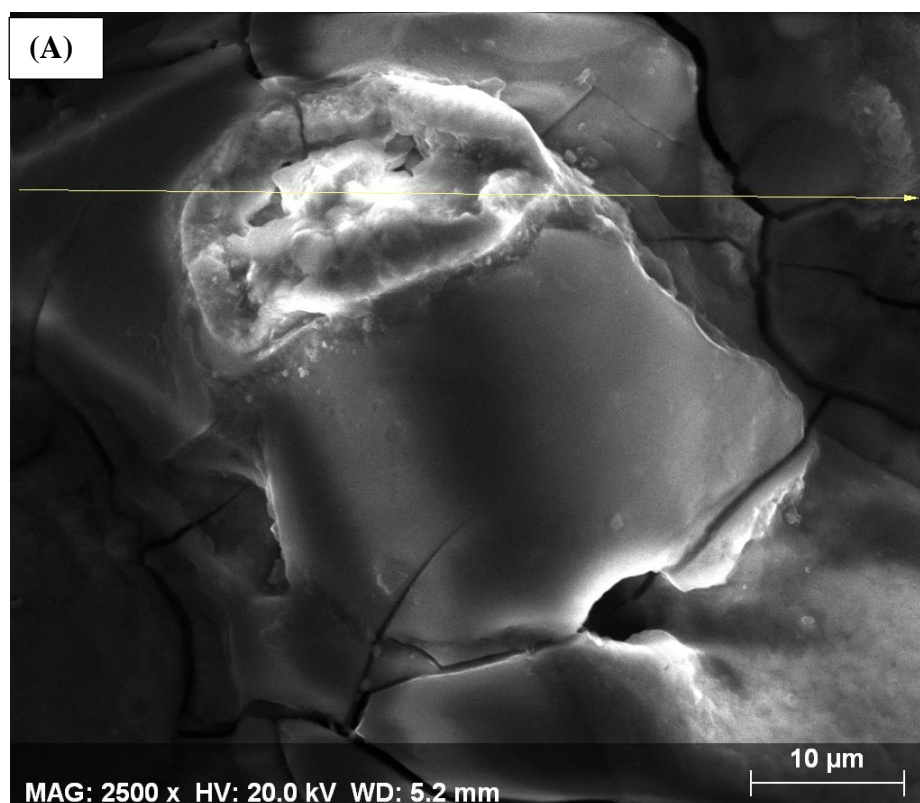
Figure 11 (A & B) illustrates how the formation of microcracks facilitated the eventual ductile fracture which in a good agreement with the results obtained Sudhakar [25].

The SEM line scans were carried out across the inclusion/steel – interface, in order to detect the composition at the inclusion. It was observed an increment of Cr signal intensity and a decrease of Cl and S signal intensity at the steel/inclusion-interface. Fig 12 indicates depletion of Cr and

accumulation of S and Cl as the scanning approached from the inclusions to the inclusion/steel interface.

The present results are in accordance with the observations which detect Cr-depletion around inclusions [26]. The signal intensity of Cr around inclusion remains strong compared to Mn signal. This strong peak of Cr however indicates to the formation of either chromium carbide or chromium sulfide. The formation of these phases is thermodynamically possible only at relatively high temperature, e.g., chromium carbide and chromium sulfide are formed at 550 - 950 and 1400 °C, respectively. These high temperatures were not applicable during the operation and welding processes. Therefore, the formation of both chromium carbide or sulfides is out of the scenario.

Combination of Figure 12 and Figure 13 demonstrate that the crack initiates from the active pit sites at which the Cl⁻ concentration is high which is an indicative of CLSCC as was outlined by Yin et al. [27]. Rate of dissolution of MnS inclusion as the origin of pit and corresponding crack growth rate at pits was observed to be faster than the overall corrosion rate, which is in a good agreement of Fantechi's results [28]. Moreover, Elsariti and Ftirman [29] indicated the possibility and propensity of pitting and Stress Corrosion Cracking behavior of austenitic stainless steel at the room temperature as well as elevated temperature. All these evidences indicate that CLSCC is the most probable mechanism responsible for the failure event of the air cooler tube where some local small pits were formed on the internal surface of tube and became the stress concentrations sources. The constant internal stress of clamping contributes to the propagation of CLSCC, as shown in Figure 14.



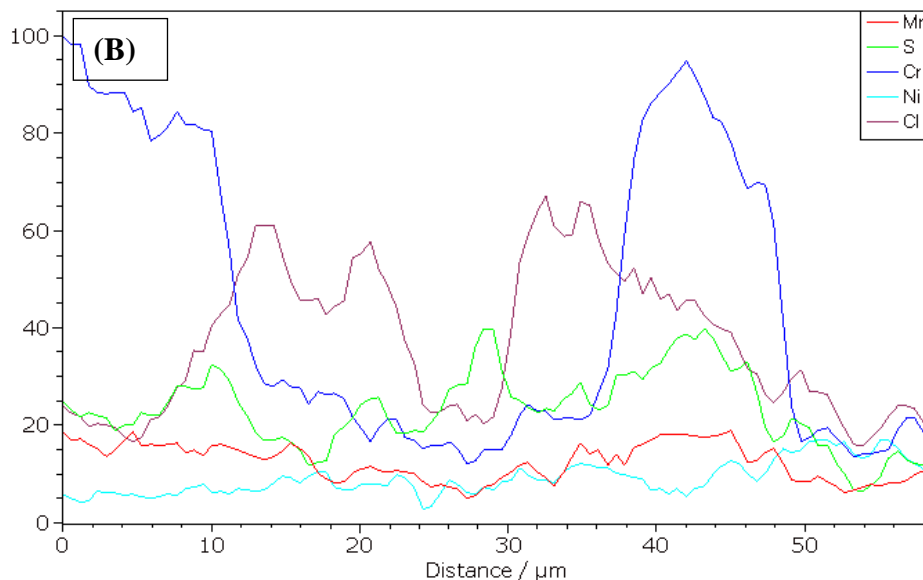
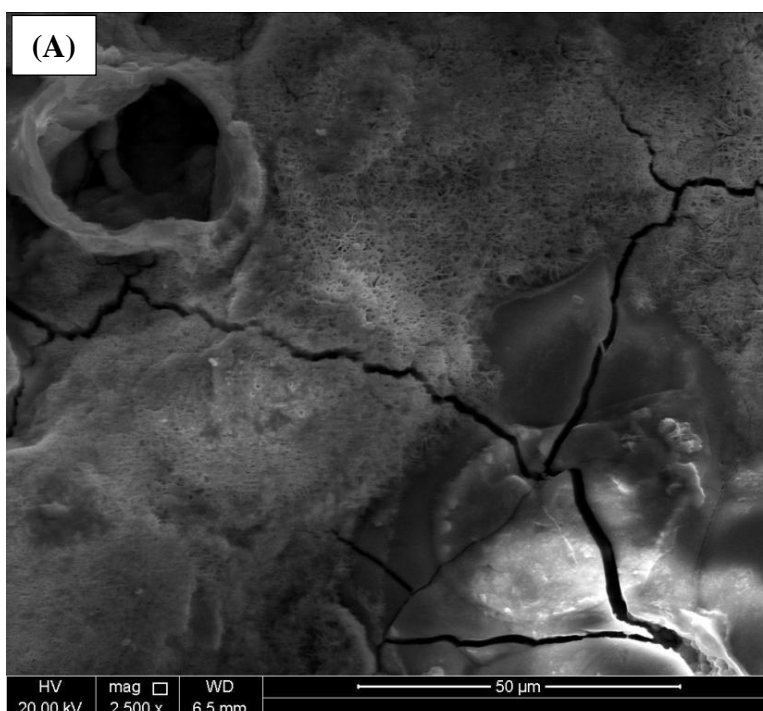


Figure 12. SEM image of an inclusion of 316L stainless steel (A) and a corresponding SEM line scan (yellow line). (B) Gives the energy-dispersive X-ray analysis of the inclusion.

It is worthy to mention that XRF proofed, See Table 1, that there were 0.3% of Cu which helped in initiating pitting corrosion, so it is recommended to have 316L SS of higher quality. Presence of Cu is favorable in terms of corrosion resistance of 316L SS when the gas stream has some H₂S in presence of Cl⁻. In this case the formed CuS will increase the corrosion resistance of the 316L stainless steel oxide layer.



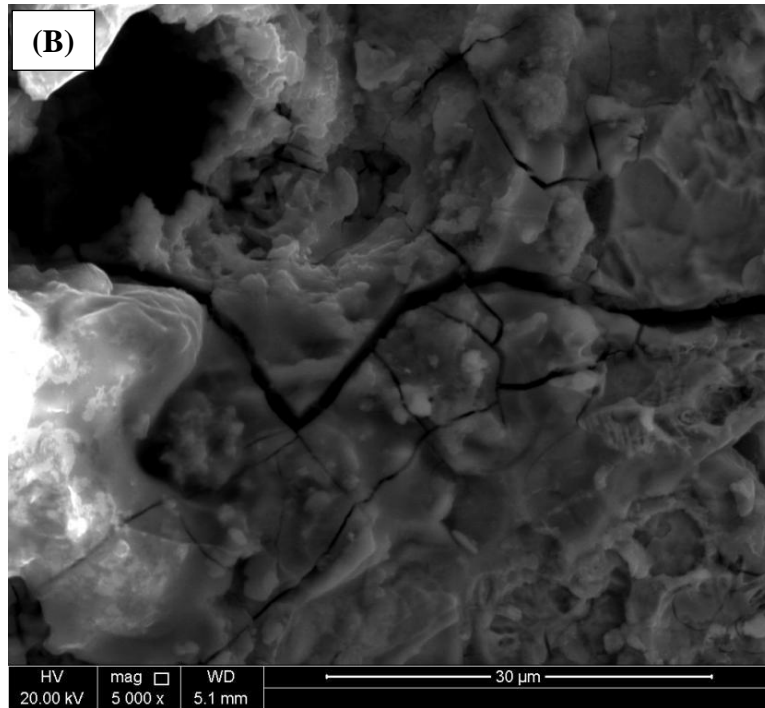
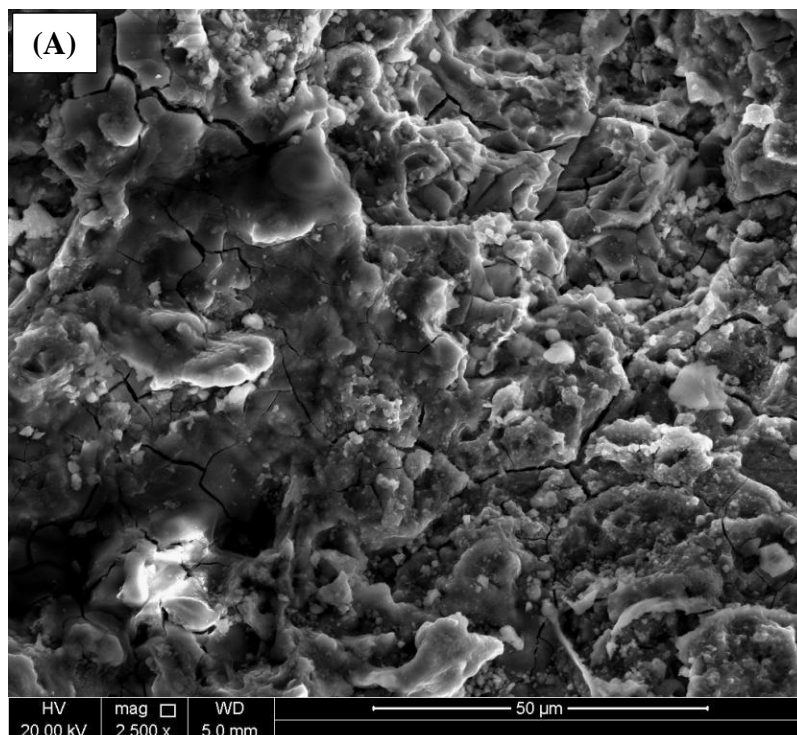


Figure 13[A and B]. SEM images illustrate the formation of pits which acted as active site for initiation of chloride stress cracking corrosion on the outer surface of 316L stainless steel.

Since the gas stream has only Cl^- but it is totally free of H_2S because of the complete removal before it entering the chiller, the presence of this low percentage of Cu in the 316L SS alloy increased the susceptibility of pitting corrosion.



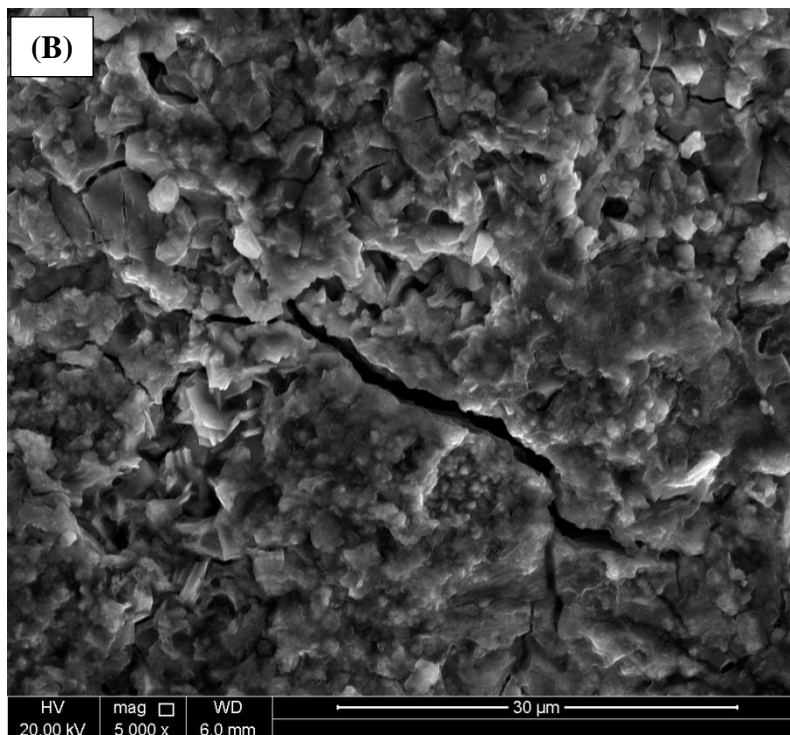


Figure 14 [A and B]. SEM images showing the formation of intensive IGC due to chloride stress cracking corrosion on inner fracture surface of 316L SS air cooler tube.

The formed pits act as stress concentrators which at the end lead to SCC. Consequently, the used 316L stainless steel must be replaced with higher quality one that is free of Cu to lower the pitting susceptibility of the alloy. It was reported that low alloying percentage of Cu increases the corrosion resistance of 316 SS in presence of chloride and H_2S but its effect is completely reversed when H_2S is absent where the corrosion rate increased dramatically [30 & 31].

4. SUMMARY AND CONCLUSIONS

The main conclusions which can be drawn from studying the failure behavior of 316L SS air chiller tube are as follow:

- The results indicate that the failure phenomenon that was primarily initiated by Cl^- led to an eventual autocatalytic pitting corrosion. The ultimate failure of the tube is concluded to be the combined effect of constant and cyclic external stress, as well as internal residual stress originated from various operating conditions.

- It is established that CLSCC is the most probable mechanism responsible for the failure event of the air cooler tube where some local small pits were formed on the internal surface of air cooler tube and became the stress concentrations sources.

- It has been verified MnS inclusions was the main initiation site for pitting in the base 316L austenitic stainless steel.

- Dissolution of the MnS inclusions induced the pit initiation process, with the contribution of released compounds from the inclusions.
- It is recommended to use higher grade of 316L SS that is free of Cu since the gas stream in the air chiller is free of H₂S. The latter, in presence of Cu, forms a CuS which increases the protection of the chromium oxide layer of 316L SS.
- Also, the removal of chlorides from the gas stream can be an option to lengthen the life time of the chiller 316L SS tubes since it will decrease the pitting corrosion rate.

ACKNOWLEDGMENTS

The authors would like to express their grateful acknowledgment for financial and in-kind support received from the Centre for Advanced Materials, (CAM), Qatar University.

References

1. C.R.F. Azevedo. *Eng. Fail. Anal.*, 14 (2007) 978–994.
2. A. Eddib, Y.A. Albrimi, A.A. Addi, J. Douch, R.M. Souto, M. Hamdani. *Int. J. Electrochem. Sci.*, 7 (2012) 6599-6610.
3. G. Meng, Y. Li, Y. Shao, T. Zhang, Y. Wang, F. Wang. *J. Mater. Sci. Technol.*, 30 (2014) 253-258.
4. Y.A. Albrimi, A. Eddib, J. Douch, Y. Berghoute, M. Hamdani, R.M. Souto. *Int. J. Electrochem. Sci.*, 6 (2011) 4614-4627.
5. M. R. Bayoumi, *Engineering Fracture Mechanics.*, 54 (1996) 879-889.
6. M. R. Bayoumi, *Bull. Faculty Engng, Assiut Univ., Egypt*, 16 (1988) 115-128
7. R.C. Yin, A.H. Al-Shawaf and W. Al-Harbi, *Engng. Fail. Anal.*, 14 (2007) 36–40.
8. B. Panda, M. Sujata, M. Madan and S.K. Bhaumik, *Engng. Fail. Anal.*, 36 (2014) 379–389.
9. C. Barbosa, J. L. Nascimento, J. L. Fernandes and I. C. Abud. *J. Fail. Anal. and Preven.*, 8 (2008) 320-326.
10. A. El-Batahgy and B. Zaghoul. *Mater. Charact.*, 54 (2005) 246– 253.
11. C.R.F. Azevedo and T. Cescon, *Análise de Falha e Metalografia. Metalografia, Casos Seleccionados (1933-2003) (Failure Analysis and Metallography, Selected Cases (1933-2003), IPT (Technology Research Institute), Sao Paulo, Brazil, 1st ed., 416 pages (2004) (in Portuguese).*
12. R. Wouters and L. Froyen, *Mater. Charact.*, 36 (1996) 357-364.
13. S. Zheng, C. Li, Y. Qi, L. Chen and C. Chen, *Corros. Sci.*, 67 (2013) 20 -31.
14. D. Peckner and M. Bernstein, *Handbook of Stainless Steels*. McGraw-Hili Book Company, New York, NY (1977).
15. Z. S. Smialowsk. *Pitting corrosion of metals*, National Association of Corrosion Engineers, Houston TX, 1986.
16. G. S. Eklund, *J. Electrochem. Soc.*, 121 (1974) 467.
17. G. Eklund, *Jernkontorets. Ann.*, 155 (1971) 637-642.
18. G. Wranglen, *Corros. Sci.*, 14 (1974) 331-349.
19. J. Stewart and D. Williams, *Corros. Sci.*, 33 (1992) 457-463, 465-474.
20. G. Butler and H. C. K. Isom, *Corrosion and its Prevention tit Water*, Robert E. Krieger, Huntington, New York (1978).
21. I. S. McCollough and A. A. Van Haute, *Corrosion.*, 30 (1971) 47-52.
22. V. Rollins, B. Arnold and E. Lardner, *J. Corrosion.*, 5 (1970) 33-45.
23. M. R. Bayoumi. *Engng. Fract. Mech.*, 45 (1993) 297-307 .

24. S. C. Srivastaya and M. B. Ives, *Corrosion*, 45 (1989) 488-493.
25. K.V. Sudhakar. *Engng. Fail. Anal.*, 12 (2005) 249–256.
26. M.P. Ryan, D.E. Williams, R.J. Chater, B.M. Hutton and D.S. McPhail, *Nature*, 415 (2002) 770.
27. R.C. Yin, A.H. Al-Shawaf and W. Al-Harbi. *Engng. Fail. Anal.* 14 (2007) 36–40.
28. F. Fantechi and M. Innocenti, *Engng. Fail Anal.* 8 (2001) 477–92.
29. S. M. Elsariti and Haftirman. *Procedia Engineering* 53 (2013) 650 – 654.
30. Akiko Tomio, Masayuki Sagara, Takashi Doi, Hisashi Amaya, Nobuo Otsuka, Takeo Kudo, *Corros. Sci.* 81 (2014)144 – 151.
31. A. Pardo, M.C. Merino, M. Carboneras, A.E. Coy, R. Arrabal, *Corros. Sci.* 49 (2007) 510 – 525.

© 2015 The Authors. Published by ESG (www.electrochemsci.org). This article is an open access article distributed under the terms and conditions of the Creative Commons Attribution license (<http://creativecommons.org/licenses/by/4.0/>).